Sensitivity of ocean heating rate estimate to time series processing methods

Jiaxin Guo[1,2,3], Lijing Cheng[*2,3], Yuying Pan[2,3], Huayi Zheng[2,3], Zhaohai Ma[*1]

[1] *China University of Geosciences Beijing.100083*

[2] *State Key Laboratory of Earth System Numerical Modeling and Application, Institute of Atmospheric Physics, Chinese Academy of Sciences, Beijing, China, 100029.*

[3] *University of Chinese Academy of Sciences, Beijing, China. 100049.*

[*]Corresponding author: Lijing Cheng: chenglij@mail.iap.ac.cn and Zhaohai Ma: zhaohaima@cugb.edu.cn

To be submitted to *Advances in Atmospheric Sciences*

https://doi.org/10.1007/s00376-026-5806-1

Abstract

Ocean heat content (OHC) is a key indicator of global warming, and OHC rate can be used to quantify Earth's energy imbalance (EEI) as ~90% of EEI is stored in the ocean. However, when estimating global ocean heating rate that is the first derivative of OHC (dOHC/dt), various time series processing methods were used, including smoothing, differentiation, and annual mean definition, which introduced differences in the resultant dOHC/dt estimate. This study utilized nine OHC datasets to analyze the impact of the above-mentioned approaches on dOHC/dt estimation and compared with the EEI observation at the top of atmosphere. The results show that the choice between the January-December and July-June annual means introduces 14% relative trend uncertainty into the estimation of the long-term trend of dOHC/dt. Different time derivative methods affect the interannual signal phase and amplitude, where the center difference for dOHC/dt and Clouds and the Earth's Radiant Energy System (CERES) strongest EEI consistency. The smoothing process further enhanced the consistency between dOHC/dt and CERES. These results indicate that the choice of time series processing techniques introduces a non-negligible uncertainty in the OHC-based EEI estimate. Moreover, this study shows that different OHC datasets show larger differences compared with the methodology choices, suggesting the data uncertainty is still the primary source of OHC-based EEI estimation errors. This study provides a methodological basis for improving EEI estimation and also for the evaluation of

climate models with observations.

Key words: EEI; OHC; Differentiation; Smoothing

Article Highlights:

- Smoothing greatly improves correlation between OHC-EEI and CERES-EEI, especially usingthe Lanczos filter.
- The July-June annual mean definition enhances consistency between OHC-based EEI and CERES-EEI compared to the calendar-year mean.
- Different choice of OHC datasets lead to larger EEI difference than time-series processing methods.

1. Introduction

Earth energy imbalance (EEI) is a crucial metric for climate change, representing the difference between net solar incoming radiation and outgoing longwave radiation at the top of the atmosphere (TOA) (Meyssignac et al., 2019; von Schuckmann et al., 2016). Under the influence of human activities, particularly greenhouse gas emissions, the Earth's energy budget at the TOA has become imbalanced (Hansen et al., 2011; Johnson et al., 2021; Trenberth et al., 2009). When EEI is positive, it indicates that the Earth system absorbs more energy than it radiates back to space, leading to continuous heat accumulation and consequent global warming. Approximately 90% of this excess energy resulting from EEI is absorbed by the ocean, primarily manifested as a sustained increase in ocean heat content (OHC) (von Schuckmann et al., 2023). Thus, changes in OHC have become one of the most widely used method for estimating EEI (Meyssignac et al., 2019). Accurate quantification of OHC and EEI is of fundamental importance for assessing climate change impacts, evaluating the effectiveness of emission reduction policies, and evaluating climate models (Cheng et al., 2022a; L'Ecuyer et al., 2015; Meyssignac et al., 2019).

Current OHC estimates still have considerable uncertainties. Firstly, the OHC estimation based on in situ observations is affected by irregular coverage of historical data and instrument bias (Abraham et al., 2013; Cheng et al., 2018; Domingues et al., 2008; Gouretski et al., 2007; Lyman et al., 2010; Rhein et al., 2013; Trenberth et al., 2016; von Schuckmann et al., 2014). Geodetic approach provides an indirect approach

of calculating OHC from altimetry and GRACE satellite missions (Hakuba et al., 2021; Meyssignac et al., 2019). Although this method can provide global coverage, its observation ability in sea ice area is limited, and is restricted by geophysical correction error and uncertainties from the thermal expansion coefficient (Ablain et al., 2019; Caron et al., 2018; Hakuba et al., 2021; Kuhlbrodt et al., 2012; Wiese et al., 2016). In addition, there are notable differences among reanalysis products in the estimation of OHC (Hakuba et al., 2024; Meyssignac et al., 2019; Palmer et al., 2015; Storto et al., 2015). Because of the above-mentioned data and technique differences, there are substantial uncertainty in calculating EEI (dOHC/dt) from OHC time series. A recent community effort (Hakuba et al., 2024) found that EEI uncertainty varied significantly among different products. The estimated ocean heat uptake (OHU) rate shows a large range, from 0.40 ± 0.12 to 0.96 ± 0.08 W m^{-2}, over the period from 2005 to 2019. W m^{-2}Moreover, the spread of the OHU rate is also large, from -0.03 ± 0.13 W m^{-2} $decade^{-1}$ to 1.1 ± 0.6 W m^{-2} $decade^{-1}$ (Hakuba et al., 2024).

Disclosing the source of errors in OHC and improving the understanding of EEI become a critical research area. Besides the above-mentioned uncertainty sources, one source of error is not fully investigated yet: the differences in data processing methods, including the way of calculating differences, the choice between time sampling and smoothing processing. These differences in processing methods may have a significant impact on the results of deriving EEI (dOHC/dt) from OHC time series, and thus become an important source of error. Some aspects of the impacts were already

revealed in previous studies. For instance, Trenberth et al. (2016) conducted one-sided difference calculations on the monthly rate of change of multiple OHC products based on Argo data and found that the standard deviation of monthly dOHC/dt -based EEI time series without smoothing was 10-13 W m^{-2}, much higher than the EEI variation of 0.64 W m^{-2} observed by CERES. Applying a 12-month moving average for smoothing significantly knocked down the noises and bring the dOHC/dt variation (0.91~1.62 W m^{-2} among different products) closer to CERES variance than using the original monthly time series. In contrast, Loeb et al. (2021)employed an overlapping annual center difference method on the OHC data (by calculating differences between year-long OHC anomalies at half-year intervals) and resulted an EEI trend estimate of 0.43 ± 0.40 W m^{-2} $decade^{-1}$ which was statistically indistinguishable from the satellite-observed trend of 0.50 ± 0.47 W m^{-2} $decade^{-1}$. Similarly, in a comparison of 21 OHC datasets, Hakuba et al. (2024) found that data processing methods significantly impact OHU estimates. Their analysis of 13 products revealed that using the cross-year mean (Jul.–Jun.), as opposed to the calendar year mean, improved the correlation between dOHC/dt and CERES EEI across most products, with one product showing a maximum increase of +0.19.

To investigate the sensitivity of dOHC/dt estimates to time series processing methods, this study uses nine OHC datasets to examine the effects of annual mean definitions, differencing methods, and smoothing techniques on the results. Furthermore, root-mean-square error (RMSE) and correlation analysis are used to

assess how these processing choices influence the consistency between dOHC/dt and CERES-EEI. Given that differencing can amplify noise in the datasets, the CERES-EEI data are integrated for comparison with OHC. Additionally, the dominant sources of uncertainty in current dOHC/dt estimates are examined. This manuscript is organized as follows: Section 2 describes the datasets used and data processing methods. Section 3 presents the results, illustrating the impacts of smoothing, differencing, annual mean definition, and monthly processing approaches on dOHC/dt estimation, and attributes the primary sources of uncertainty. Section 4 contains conclusion and discussion.

2. Data and Method

2.1 Data

This study selected nine global OHC datasets (Table 1), covering various observational sources and processing methods to ensure the comprehensiveness of the analysis and the reliability of the conclusions. The dataset includes five data sets based on in situ observations, two reanalysis products, one product based on satellite sea level height reconstruction, and one product integrating multi-source observations and models. The in situ observations of OHC are from the following data sets EN4 (Good et al., 2013), Scripps Institution of Oceanography (SIO) (Roemmich et al., 2009), Institute of Atmospheric Physics (IAP , version 4.2) (Cheng et al., 2024; Cheng et al., 2017; Cheng et al., 2016), Japan Agency for Marine-Earth Science and Technology (JAMSTEC) (Hosoda et al., 2008), Ishii (Ishii et al., 2017). Two reanalysis products

include Estimating the Circulation and Climate of the Ocean (ECCO, version 4) (Forget et al., 2015) and Ocean Reanalysis System 5 (ORAS5) (Zuo et al., 2019). The product based on satellite sea-level height reconstruction is from the Laboratoire d'Etudes en Géophysique et Océanographie Spatiales (LEGOS) (Marti et al., 2022). The dataset integrating multi-source observations and models is sourced from the Pacific Marine Environmental Laboratory (PMEL) in the United States, specifically from the Random Forest Regression Ocean Maps (RFROM) analysis system (Lyman et al., 2023). These datasets vary significantly in terms of spatial resolution, observation methods, and error structure, providing diverse test conditions for the comparison of different processing methods. Observations after 2005 and ocean depths 0-2000 m were used in this study, mainly because the Argo network achieves near-global open ocean coverage, which significantly improves the quality and consistency of OHC and makes EEI analysis more reliable.

The net TOA radiation fluxes are obtained from the Clouds and the Earth's Radiant Energy System Energy Balanced and Filled (CERES-EBAF) dataset, version 4.2 (Loeb et al., 2018). The CERES instrument suite is composed of wide-band radiometers carried by multiple satellites, designed to precisely measure the Earth's radiation budget. Since March 2000, the CERES instrument has been continuously operating on satellite platforms such as Tropical Rainfall Measuring Mission (TRMM), Terra, Aqua, Suomi National Polar-orbiting Partnership (S-NPP) and National Oceanic and Atmospheric Administration 20 (NOAA-20), accumulating over two decades of global shortwave

and long-wave radiation data. The EBAF processing ensures consistency between the CERES observations and energy balance constraints by applying bias corrections and energy balance adjustments, thereby yielding radiation fluxes that are widely regarded as the benchmark for Earth's radiation budget studies. The EBAF-TOA-Level 3b product employed in this study provides monthly mean incoming solar radiation, TOA fluxes (including short-wave, long-wave radiation fluxes and net fluxes), and cloud parameter products based on CERES-MODIS inversion at a spatial resolution of 1°×1°. Through time integration and calibration, the dataset also delivers consistent long-term radiation flux time series that are widely used to assess the Earth's radiation budget and energy imbalance. In this study, we selected the period from January 2005 to October 2023 as the analysis period to match the observation cycle of changes in ocean heat absorption.

Table 1. Description of the datasets used in this study.

Product name	Time range	Spatial range	Time resolution	Spatial resolution	Interpolation method
objective analysis data					
IAPv4	1940-Present	Global	Monthly	1°×1°	Ensemble Optimal Interpolation with dynamic ensemble
Ishii	1955-2024	Global	Yearly	1°×1°	3-D Variational Approach
EN4	1900-Present	Global	Monthly	1°×1°	Optimal Interpolation (using the Analysis Correction scheme)
SIO	2004-Present	Global	Monthly	1°×1°	Weighted Least-Squares Fit + Objective Analysis
JAMSTEC	2001-2022	Global	Monthly	1°×1°	Optimal

					interpolation
reanalysis data					
ECCO	1992-2024	Global	Monthly	0.5°×0.5°	4D Variational Data assimilation approach
ORAS5	1979-present	Global	Monthly	1°×1°	3D Variational Data assimilation approach
Satellite-based data					
LEGOS	2002-2020	Global	Monthly	3°×3°	Altimetry sea level, GRACE
CERES	2000-2025	Global	Monthly	1°×1°	TOA radiation
fused data					
PMEL RFROM	1993-2024	Global	Monthly	0.25°×0.25°	Machine learning (Random Forest Regression)

2.2 Method

To investigate the sensitivity of dOHC/dt estimates to time series processing methods, this study designed and compared several workflows. These workflows combine established methods from the literature with new approaches introduced for this analysis. For clarity, all processing strategies are summarized in Table 2. The individual steps involved, including time series type, smoothing, and differentiation, are detailed in the subsequent sections.

The time series processing methods selected in this study are intended to cover the most commonly used and representative categories of techniques in the literature. The forward, central, and backward difference methods are the three fundamental building blocks of finite differencing. The choice of smoothing methods encompasses a range from simple n-point moving averages (MA, WMA) to commonly used filters with high frequency response characteristics, such as the Butterworth and Lanzcos filters, all of

180 which are widely applied in classical oceanographic and climate data analysis (e.g.,
181 Hakuba et al., 2024; Trenberth et al., 2016). The calendar-year and cross-year annual
182 mean definitions are the two most discussed schemes in the current community.
183 Therefore, the analytical framework of this study aims to systematically quantify the
184 sensitivity of dOHC/dt estimates to these selected and representative processing
185 methods.

186 **Table 2.** Summary of time series processing methods for dOHC/dt estimation
187 examined in this study.

ID	Time Series Type	Smoothing Method	Differentiation Method	Reference
1	Monthly	13-month moving average (with end weights of 0.5)	Center difference	Smoothing based on (Trenberth et al., 2016)
2	Monthly	25-month moving average (with end weights of 0.5)	Center difference	
3	Annual (Calendar Year /Cross Year)	None (RAW)	Center difference	
4	Annual (Calendar Year /Cross Year)	Moving average (3-year)	Center difference	Smoothing based on (Abraham et al., 2013)
5	Annual (Calendar Year /Cross Year)	Non-equal-weighted moving mean (0.5-1-0.5) (3-year)	Center difference	
6	Annual (Calendar Year /Cross Year)	Lanzcos filter (3-year cutoff)	Center difference	Smoothing based on (Hakuba et al., 2024)
7	Annual (Calendar Year /Cross Year)	Butterworth filter (3-year)	Center difference	(Roberts et al., 2017)

8	Annual (Calendar Year /Cross Year)	None (RAW)	Forward difference	
9	Annual (Calendar Year /Cross Year)	Moving average (3-year)	Forward difference	Smoothing based on (Abraham et al., 2013)
10	Annual (Calendar Year /Cross Year)	Non-equal-weighted moving mean (0.5-1-0.5) (3-year)	Forward difference	
11	Annual (Calendar Year /Cross Year)	Lanzcos filter (3-year cutoff)	Forward difference	Smoothing based on (Hakuba et al., 2024)
12	Annual (Calendar Year /Cross Year)	Butterworth filter (3-year)	Forward difference	Smoothing based on (Roberts et al., 2017)
13	Annual (Calendar Year /Cross Year)	None (RAW)	Backward difference	
14	Annual (Calendar Year /Cross Year)	Moving average (3-year)	Backward difference	Smoothing based on (Abraham et al., 2013)
15	Annual (Calendar Year /Cross Year)	Non-equal-weighted moving mean (0.5-1-0.5) (3-year)	Backward difference	
16	Annual (Calendar Year /Cross Year)	Lanzcos filter (3-year cutoff)	Backward difference	Smoothing based on (Hakuba et al., 2024)
17	Annual (Calendar Year /Cross Year)	Butterworth filter (3-year)	Backward difference	Smoothing based on (Roberts et al., 2017)

2.2.1 Smoothing

This study tested multiple smoothing methods to evaluate the impact of suppressing high-frequency noise on dOHC/dt estimation. For annual-mean time series, four methods were compared: the Lanczos low-pass filter (3-year cutoff period)

(Hakuba et al., 2024), a 3-point weighted moving average (WMA, weights 0.5-1-0.5), a 3-year simple moving average (MA) (Abraham et al., 2013), and the Butterworth low-pass filter (3-year cutoff period) (Roberts et al., 2017). Furthermore, for comparison with the annual processing workflow, two smoothing methods applied directly to monthly time series were introduced, both following the approach of (Trenberth et al., 2016): one is their proposed 13-month running mean (with end weights of 0.5), and the other is an extended 25-month running mean (with end weights of 0.5) designed to further suppress interannual variability.

2.2.2 Differentiation

Three differential methods are used to calculate the time derivative of OHC (dOHC/dt):

$$\left.\frac{\mathrm{d}OHC}{\mathrm{d}t}\right|_{t=t_i} = \begin{cases} \dfrac{OHC(t_i+\Delta t)-OHC(t_i)}{\Delta t}, & Forward\quad difference \\ \dfrac{OHC(t_i+\Delta t)-OHC(t_i-\Delta t)}{2\Delta t}, & Center\quad difference \\ \dfrac{OHC(t_i)-OHC(t_i-\Delta t)}{\Delta t}, & Backward\quad difference \end{cases}$$

Where $OHC(t_i)$ is the OHC at time t_i, $\left.\frac{\mathrm{d}OHC}{\mathrm{d}t}\right|_{t=t_i}$ is the rate of change of OHC at time t_i, and Δt is the time interval between two adjacent records.

In this study, the above three difference methods were applied to the processed OHC time series to calculate dOHC/dt. The time step (Δt) is determined by the inherent time resolution of the final smoothed sequence. Therefore, for the annual time series, Δt is one year; For the monthly time series, Δt is one month. The OHU time

series data is derived from the time derivative calculation of OHC and is ultimately normalized through the area of the top of the atmosphere (TOA) at a height of 20 kilometers on the Earth's surface, which is 5.14×10^{14} square meters.

2.2.3 Annual mean definition

This study used two definitions to define annual mean: January-December mean and July-June mean. The later consider the influence of El Niño-Southern Oscillation (ENSO),which always peaks at winter (Rasmusson et al., 1982).

2.2.4 Comparison with CERES

Because doing the time derivative will certainty amplify the noise in data, this study also performed an additional comparison between OHC and EEI: doing the time integration of CERES net radiation flux data to obtain the cumulative energy series, and remove the linear trend and then compare the result with de-trended OHC time series for their inter-annual to decadal scale changes. To derive the ocean warming acceleration, we performed quadratic polynomial fitting on OHC.

To quantify the differences between the processed dOHC/dt sequence and the CERES EEI sequence, this study adopts the Pearson correlation coefficient (R) and root mean square error (RMSE) as two key metrics:

$$R = \frac{\sum_{i=1}^{n}(r_i - \overline{r})(s_i - \overline{s})}{\sqrt{\sum_{i=1}^{n}(r_i - \overline{r})^2 \sum_{i=1}^{n}(s_i - \overline{s})^2}}$$

$$RMSE = \sqrt{\frac{1}{n}\sum_{i=1}^{n}(r_i - s_i)^2}$$

Where r_i represents the warming rate (OHU) at different time points calculated

by various methods, s_i denotes the processed CERES radiative values at corresponding time steps, $\overline{r}$ is the mean of r_i and $\overline{s}$ is the mean of s_i.

Within the framework of this study, these two indicators were employed to assess different aspects of consistency. The RMSE mainly quantifies the average magnitude of the absolute error between two time series at each time point. While the Pearson correlation coefficient (r) mainly measures the similarity in the form and phase consistency of the interannual fluctuations of the two sequences. By combining the use of these two indicators, the consistency of the estimated dOHC/dt results in terms of numerical deviation and temporal evolution pattern with CERES can be simultaneously evaluated.

3. Results

3.1 Smoothing Method Sensitivity

The choice of smoothing method affects the estimation of dOHC/dt, including its interannual variability and long-term trend. Figure 1a compares the dOHC/dt anomaly series after applying different smoothing methods to various datasets. Taking the Ishii dataset as an example (Figure 1a), the values of the dOHC/dt anomaly series processed by different smoothing methods can differ by up to 0.53 W m^{-2} in peak years such as 2008. The smoothing differences results in an estimated linear trend for 2005–2024 ranging from 0.27 to 0.29 W m^{-2} $decade^{-1}$. Further analysis across all datasets shows that applying a series of smoothing treatments reduces the interannual standard deviation of dOHC/dt by an average of 0.07 W m^{-2} (Table 3) compared to the unsmoothed RAW series, indicating the suppressive effect smoothing on interannual

252 variability.

253 At the same time, the choice of smoothing method (including RAW series) alone
254 introduces an average uncertainty (measured by standard deviation) in the estimated
255 long-term trend of 0.02 W m^{-2} $decade^{-1}$ (Table 4). Relative to the overall mean trend
256 (0.33 W m^{-2} $decade^{-1}$) across all datasets and smoothing methods, this difference
257 constitutes approximately 6% relative uncertainty, which is important for accurately
258 assessing the Earth's energy budget. Among all datasets, the trend estimation for ECCO
259 shows the highest sensitivity (standard deviation = 0.05) to the choice of smoothing
260 method, while ORAS5 shows the lowest sensitivity. These results indicate that the
261 choice of smoothing method is a source of uncertainty that should be quantified in the
262 estimation of the long-term trend of dOHC/dt.

263

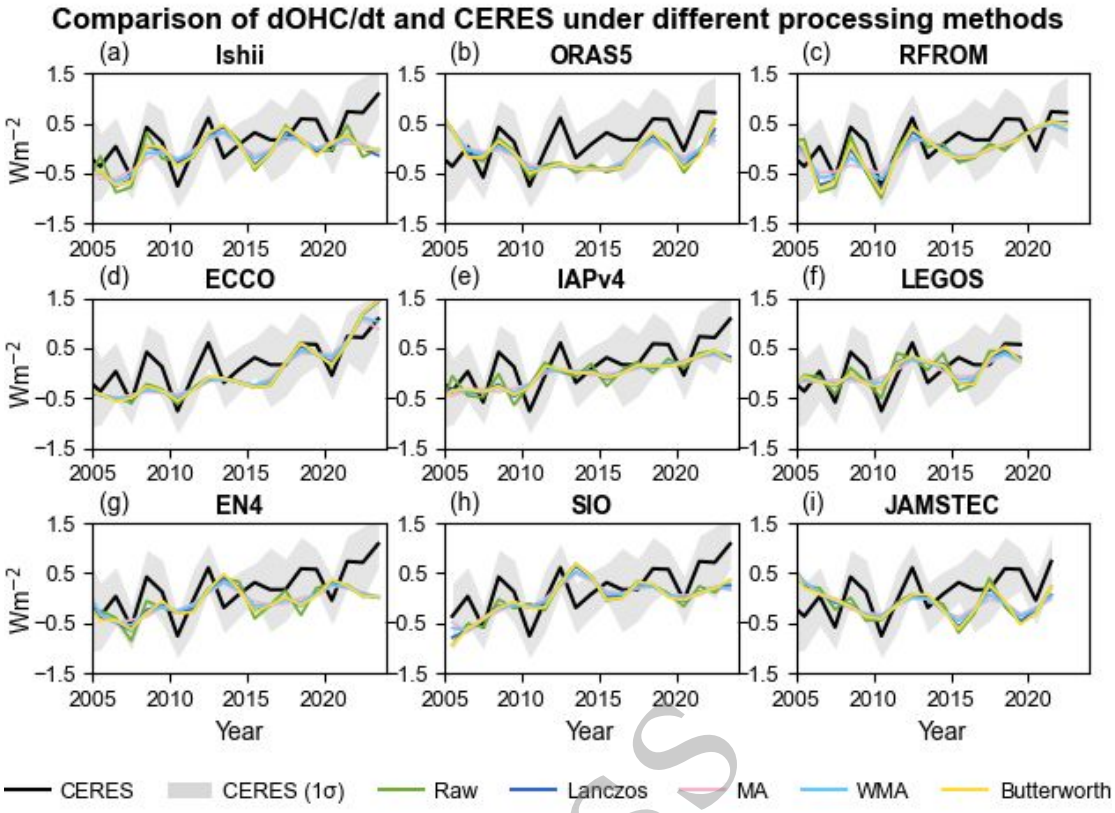

Figure 1. Impacts of different smoothing methods on dOHC/dt calculation compared with CERES data after central differencing. Each panel represents a OHC dataset. Different lines correspond to various smoothing methods and the solid black line represents results from CERES data, with the gray shaded area indicating the ±1 standard deviation (±1σ) range, calculated from the 12 monthly CERES values within each year. Unit: W m^{-2}.

Table 3. Quantification of the effect of smoothing on the interannual standard deviation of dOHC/dt anomalies. Unit: W m^{-2}. "Std Dev (RAW)" is the standard deviation of the original sequence; "Mean Std Dev (Smoothed)" is the arithmetic mean of the standard deviations obtained after each dataset is processed by four smoothing

276 methods respectively. "Reduction" is listed as the difference between the two. The
277 interannual standard deviation of CERES-EEI is 0.48 W m^{-2}.

Dataset	Std Dev (RAW)	Mean Std Dev (Smoothing)	Reduction
Ishii	0.37	0.29	0.08
ORAS5	0.32	0.26	0.06
RFROM	0.45	0.36	0.09
ECCO	0.57	0.52	0.05
IAPv4	0.29	0.25	0.04
LEGOS	0.32	0.22	0.10
EN4	0.31	0.26	0.05
SIO	0.38	0.33	0.05
JAMSTEC	0.29	0.22	0.07
Average	**0.37**	**0.30**	**0.07**

278

279 **Table 4.** Quantification of uncertainty in dOHC/dt trend estimates (W m^{-2} $decade^{-1}$)
280 arising from the choice of smoothing method.

Dataset	Trend MA3	Trend WMA3	Trend Lanzcos	Trend Butterworth	Trend Uncertainty
Ishii	0.27	0.27	0.29	0.29	0.01
ORAS5	0.05	0.05	0.06	0.06	0.01
RFROM	0.50	0.51	0.56	0.53	0.03
ECCO	0.78	0.81	0.89	0.89	0.05
IAPv4	0.38	0.38	0.41	0.40	0.01
LEGOS	0.29	0.30	0.33	0.34	0.02
EN4	0.29	0.29	0.31	0.31	0.01
SIO	0.36	0.38	0.42	0.44	0.04
JAMSTEC	-0.09	-0.09	-0.11	-0.09	0.01
Average	**0.30**	**0.31**	**0.35**	**0.36**	**0.02**

On the other hand, in the comparison between OHC-based EEI and CERES-EEI, the positive role of smoothing is mainly reflected in the improvement of correlation. The time series (Figure 1a) shows that the smoothed OHC-based EEI from various datasets exhibits better agreement with CERES-EEI in certain years than the raw time series. For instance, in 2008, most OHC datasets under different smoothing methods show large positive EEI values, corresponding to the high value observed by CERES in that year. However, noticeable discrepancies remain in some periods. For example, while CERES observations show a significantly high EEI value in 2015, none of the OHC datasets reproduce this enhanced signal. To quantitatively evaluate these observations, Figure 2 presents the RMSE and Pearson correlation coefficient between dOHC/dt and CERES-EEI.

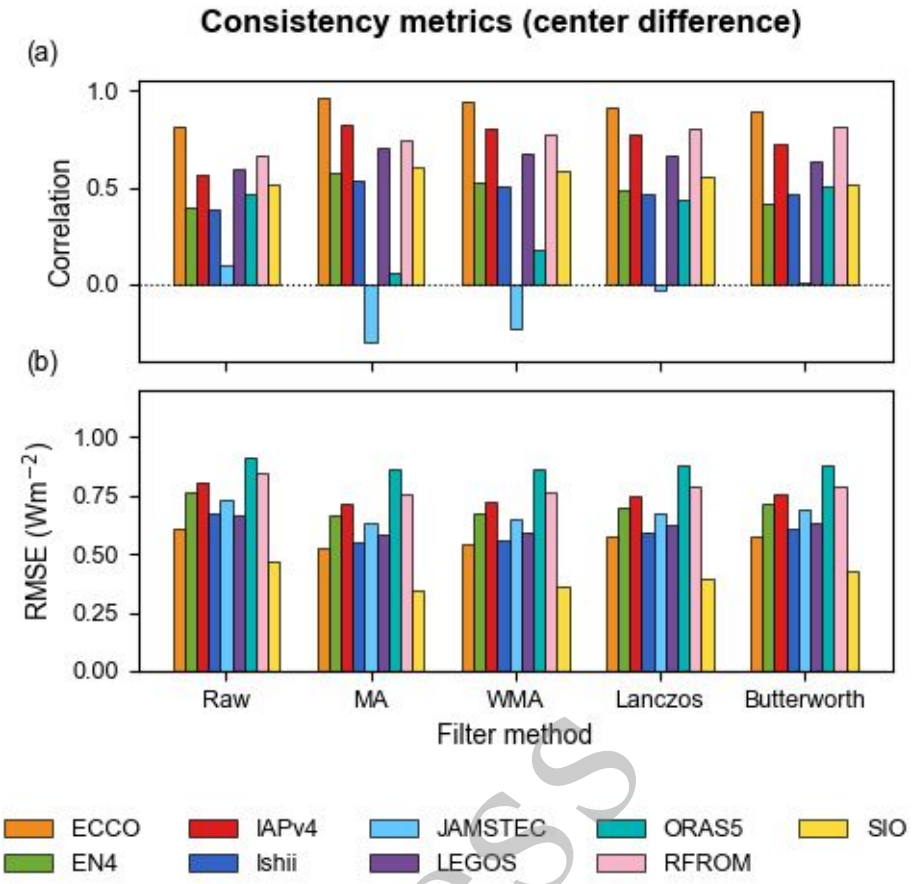

294

295 **Figure 2.** Quantitative comparison of dOHC/dt estimates with CERES-EEI, showing
296 the impacts of different smoothing methods and datasets. a) the Pearson correlation
297 coefficients and b) the Root Mean Square Error (RMSE) in W m^{-2}.

298

299 Quantitative analysis of RMSE (Figure 2b) indicates that smoothing had a limited
300 impact on reducing the overall error level between OHC-based EEI and CERES-EEI.
301 On average, across the nine datasets, applying smoothing reduced the RMSE by only
302 0.07 W m^{-2} on average compared to the unsmoothed RAW series (Table 5). Unlike the
303 stability of RMSE, the Pearson correlation coefficient showed sensitivity to the choice
304 of smoothing method (Figure 2a). All smoothing methods improved the correlation
305 between OHC-based EEI and CERES-EEI to varying degrees. The results show that

306 compared to the RAW series (mean r = 0.55), smoothing increased the mean correlation
307 coefficient to above 0.62 (excluding the JAMSTEC outlier). Among the methods, the
308 Lanczos filter produced the most notable average improvement, systematically
309 increasing the mean correlation coefficient to 0.64. The Lanczos and Butterworth filters
310 demonstrated relatively stronger stability in enhancing correlation, maintaining it above
311 0.4 for most datasets (except JAMSTEC) and avoiding extreme outcomes like those
312 sometimes seen with MA. However, no single method achieved optimal results under
313 all circumstances.

314 **Table 5.** Quantification of the effect of smoothing on the RMSE between dOHC/dt
315 anomalies and the CERES-EEI reference. Unit: W m^{-2}.

Dataset	RMSE(RAW)	Mean RMSE (Smoothing)	RMSE Reduction
Ishii	0.67	0.58	0.09
ORAS5	0.91	0.87	0.04
RFROM	0.85	0.78	0.07
ECCO	0.61	0.55	0.06
IAPv4	0.81	0.73	0.08
LEGOS	0.67	0.61	0.06
EN4	0.76	0.69	0.07
SIO	0.47	0.38	0.09
JAMSTEC	0.74	0.66	0.08
Average	**0.72**	**0.65**	**0.07**

316 ***3.2 Differentiation Sensitivity***

317 The choice of differencing method introduces uncertainties in both phase and
318 amplitude of the interannual signal in dOHC/dt estimates. Figure 3a shows the dOHC/dt

results obtained by applying three different differencing methods to the unsmoothed ensemble mean series (RAW). As illustrated in Figure 3a, the choice of differencing method leads to phase shifts in the peaks and troughs of the dOHC/dt series. These phase shifts translate into instantaneous estimation differences during years with strong interannual variability. For instance, in 2007, the difference between the values calculated using forward and backward differences reached 1.4 W m^{-2}. Furthermore, in terms of the amplitude of interannual variability, both forward difference (standard deviation = 0.40 W m^{-2}) and backward difference (standard deviation = 0.43 W m^{-2}) exhibit larger amplitude fluctuations compared to the central difference (standard deviation = 0.27 W m^{-2}). Additionally, for the estimation of the long-term trend, the uncertainty in trend introduced by the choice of differencing method (measured by the standard deviation of the trend values) is 0.04 W m^{-2} $decade^{-1}$. This constitutes a relative uncertainty of approximately 14% relative to the overall mean trend (0.29 W m^{-2} $decade^{-1}$) across the different differencing methods.

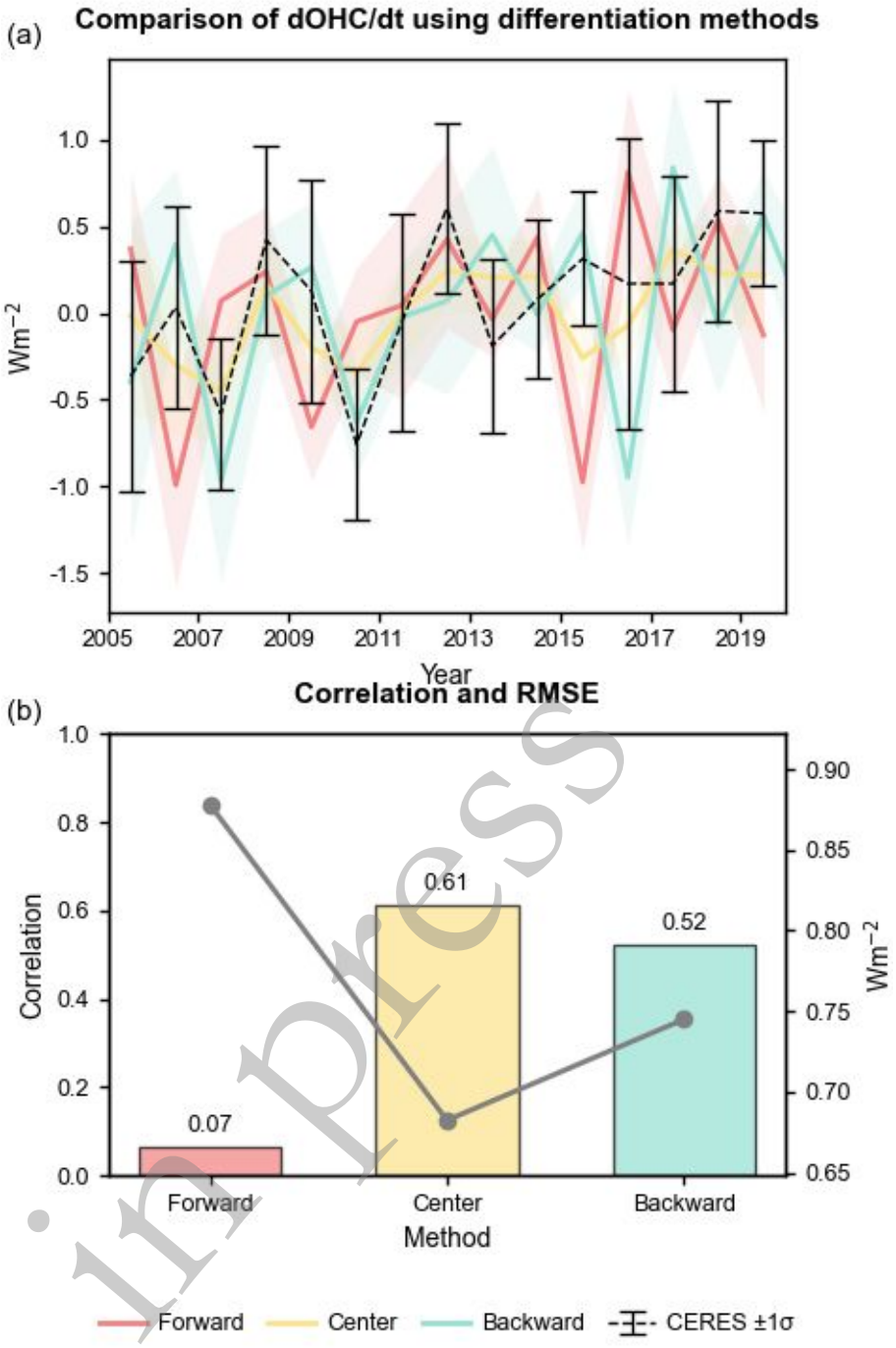

334

335 **Figure 3.** Impacts of different differentiation methods on the multi-dataset average

336 dOHC/dt and its consistency with CERES-EEI. a) Compare the time series of the multi-

337 dataset average dOHC/dt calculated using forward, center, and backward difference

338 methods. The shaded areas represent the ±1 standard deviation range across the nine

OHC datasets for each respective method. The black dashed line with error bars shows the CERES-EEI benchmark and its intra-annual ±1σ range. b) Present the quantitative comparison with CERES, showing the Pearson correlation coefficient (bars) and the RMSE in W m^{-2} (gray line) for each differentiation method. All calculations are based on the unsmoothed (Raw) calendar-year (Jan-Dec) annual mean series.

In the comparison with CERES-EEI, none of the three differencing methods fully captured the complete interannual signal variations of CERES-EEI in terms of the time series morphology (Figure 3a). To quantitatively assess this uncertainty, Figure 3b presents the Pearson correlation coefficients and RMSE between dOHC/dt and CERES-EEI for the three differencing methods. Specifically, the central difference method achieved a correlation coefficient of 0.61, which is higher than that of the backward difference (0.52) and the forward difference (0.07). Furthermore, the central difference also yielded the lowest RMSE (0.69 W m^{-2}), outperforming the backward difference (0.74 W m^{-2}) and the forward difference, which had the largest error (0.88 W m^{-2}). In summary, the forward difference introduced the largest error and the lowest correlation; the backward difference performed moderately; while the central difference demonstrated the most robust and accurate performance across all evaluation metrics. Therefore, this study selects the central difference method as the standard computational approach for all subsequent work.

3.3 Annual Mean Definition Sensitivity

Figure 4 compares the ensemble mean dOHC/dt series obtained using different smoothing methods under the calendar year (January–December) and cross-year (July–June of the following year) averaging definitions. Comparison reveals that the choice of annual averaging definition alters the phase and shape of the interannual signal in dOHC/dt. For instance, under the calendar year average (Figure 5a), the mean curve from all datasets forms a peak during the 2016–2017 period, whereas under the cross-year average (Figure 5b), this period exhibits a flat trend. Quantifying the amplitude shows that using the cross-year average reduces the interannual standard deviation of the ensemble mean (RAW) series from 0.25 W m^{-2} (calendar year) to 0.22 W m^{-2}. This suggests that the cross-year averaging definition, by aligning with the natural cycles of key climate modes such as ENSO, physically better represents the interannual signals. Furthermore, for the estimation of the long-term trend, the uncertainty in trend introduced by the choice of annual averaging definition (measured by standard deviation) is 0.05 W m^{-2} $decade^{-1}$. This constitutes a relative uncertainty of approximately 14% relative to the overall mean trend (0.35 W m^{-2} $decade^{-1}$).

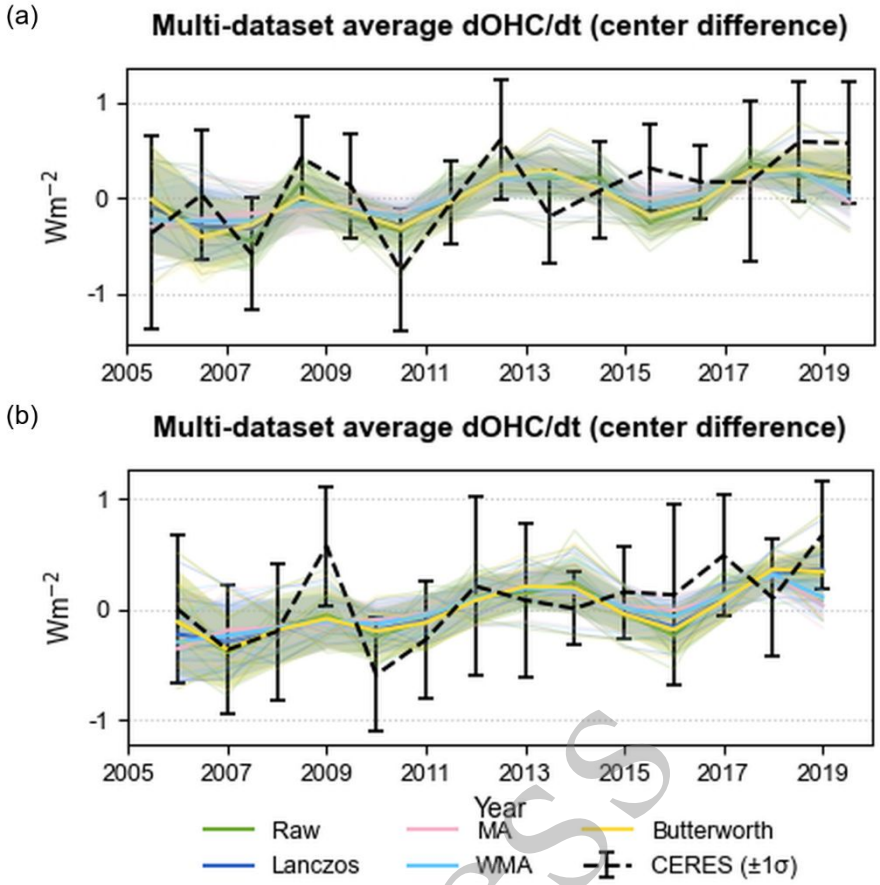

376

377

378 **Figure 4.** Impacts of different annual mean definitions on the multi-dataset average
379 dOHC/dt. a) The multi-dataset average dOHC/dt time series under the calendar-year
380 (Jan-Dec) definition. The thick colored lines represent the ensemble average for each
381 of the five smoothing methods. The thin, semi-transparent background lines show the
382 results from individual OHC datasets, and the shaded area represents their ±1 standard
383 deviation range. The black dashed line with error bars shows the CERES-EEI
384 benchmark and its intra-annual ±1σ range. b) Same as in a), but for the cross-year (Jul-
385 Jun) annual mean definition.

386

In the comparison with CERES-EEI, the time series (Figure 4) shows that during certain periods (2015–2016), the cross-year average yields better alignment between the dOHC/dt series and the CERES-EEI curve. A quantitative analysis was conducted by calculating the RMSE and Pearson correlation coefficient for the unsmoothed RAW series under different annual averaging definitions. The calculation results show that adopting the cross-year mean leads to a consistent improvement in both metrics, with the RMSE decreasing from 0.68 W m^{-2} (calendar year) to 0.67 W m^{-2}, while the Pearson correlation coefficient simultaneously increases from 0.61 (calendar year) to 0.63. W m^{-2}W m^{-2}This indicates that the cross-year average, by avoiding the truncation of interannual signals in the dOHC/dt calculation to some extent, physically reduces estimation uncertainty and thereby enhances the consistency between dOHC/dt and CERES-EEI.

3.4 Monthly Smoothing Sensitivity

In addition to processing the annual average series, this study, following the approach of (Trenberth et al., 2016), directly applies smoothing to the original monthly OHC time series: a 13-month moving average (13WMA) and an extended 25-month moving average (25WMA) for further smoothing. Figure 5 displays the dOHC/dt time series after applying these two methods to all nine datasets. The figure visually indicates that the 13WMA method retains substantial amplitude. In contrast, the 25WMA method provides stronger smoothing, reducing the mean standard deviation of the dOHC/dt

series from 1.72 W m^{-2} (13WMA) to 1.12 W m^{-2}.

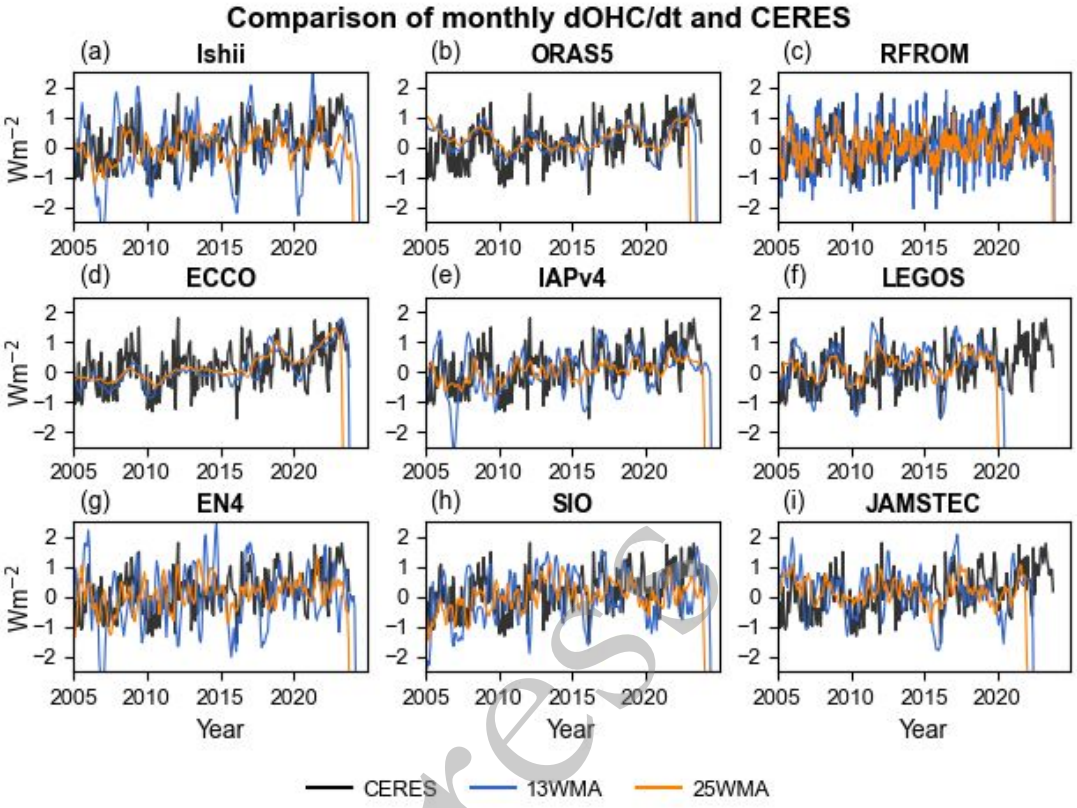

Figure 5. Impacts of different moving average windows on monthly dOHC/dt estimates, compared with monthly CERES-EEI. Each of the nine panels corresponds to a specific OHC dataset. Within each panel, the blue and orange lines represent the dOHC/dt time series calculated from the original monthly OHC data using a 13-month (13WMA) and a 25-month (25WMA) weighted moving average, respectively. The black line indicates the monthly CERES-EEI benchmark. All dOHC/dt series are calculated using central differencing.

In the comparison with CERES-EEI, the dOHC/dt series under both methods show

low coherence with the CERES-EEI series in terms of amplitude and temporal structure. To quantify this observation, Figure 6 presents the correlation coefficients and RMSE between dOHC/dt and CERES-EEI for the two methods. On average, across all nine datasets, switching from 13WMA to 25WMA reduces the mean RMSE from 1.22 W m^{-2} to 0.98 W m^{-2}. However, the stronger smoothing conversely lowers the mean correlation coefficient from 0.21 (13WMA) to 0.18 (25WMA). This suggests that the 25-month smoothing window may excessively smooth some genuine interannual signals, leading to reduced phase agreement with CERES. Overall, compared to the dOHC/dt calculated directly from monthly data, the dOHC/dt derived from annual processing demonstrates better consistency with CERES-EEI.

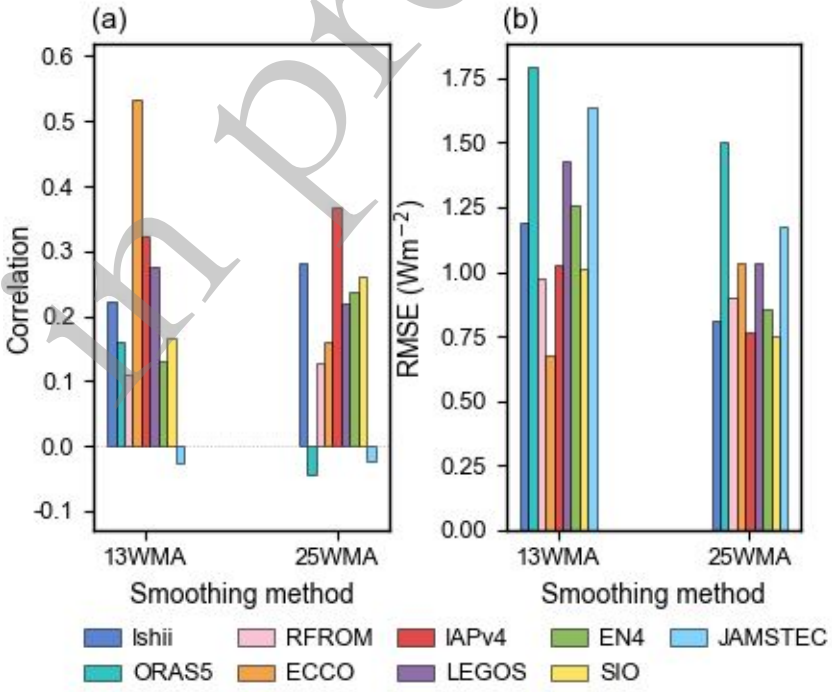

Figure 6. Quantitative comparison of monthly dOHC/dt estimates with monthly CERES-EEI. a) the Pearson correlation coefficients and b) the Root Mean Square Error

(RMSE) in W m^{-2}.

3.5 Data Sensitivity

In addition to the time series processing methods discussed in previous sections, the OHC dataset itself is also a key source of uncertainty. This central finding is most clearly demonstrated in the line chart of Figure 7, which compares the dOHC/dt and CERES-EEI time series across different datasets under a fixed methodology. The amplitude variations differ among datasets across various time periods. Results show that for the RAW series subplot (Figure 7), the interannual amplitude (measured by standard deviation) of the datasets ranges from 0.29 W m^{-2} to 0.57 W m^{-2}. Furthermore, differences exist in the signal phase across datasets. In 2013, SIO and EN4 exhibit a phase opposite to that of ORAS5. For the estimation of the long-term trend, the uncertainty in trend introduced by the choice of dataset is 0.29 W m^{-2} $decade^{-1}$, constituting a relative uncertainty of approximately 83% relative to the overall mean trend (0.35 W m^{-2} $decade^{-1}$). This indicates that the primary limiting factor for the accurate quantification of dOHC/dt is the dataset itself. The observed inter-dataset discrepancies are likely a composite of both random and systematic errors. These inconsistencies may stem from multiple factors, including differences in quality control (QC), bias correction, gap-filling techniques, and the CERES satellite instrument calibration errors.

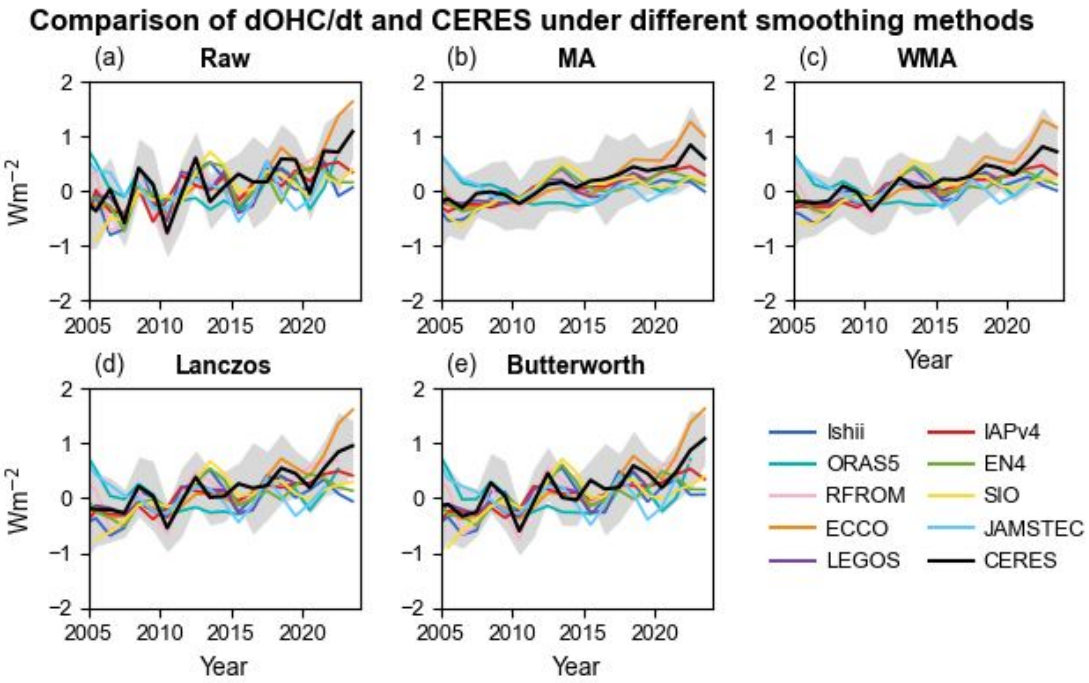

Figure 7. Inter-dataset comparison of central-differenced dOHC/dt estimates under different smoothing methods, compared with CERES-EEI. Each of the five panels corresponds to a specific smoothing method (including Raw). Within each panel, colored lines represent the dOHC/dt time series from the nine different OHC datasets, while the black line indicates the CERES-EE-I benchmark. The gray shaded area represents the intra-annual ±1σ range of the CERES data. All dOHC/dt series are based on the calendar-year (Jan-Dec) annual mean definition.

In the comparison with CERES-EEI, the amplitude and temporal structure of dOHC/dt vary across different datasets. Figure 8 shows that, overall, OHC-based EEI is consistent with CERES-EEI during certain periods (2007–2010). However, in other periods, such as 2012–2015, SIO, EN4, and Ishii exhibit energy absorption maxima that are completely opposite to the energy absorption minima of CERES-EEI, indicating

deviations. To quantify the differences among datasets, Figure 8 presents the RMSE and correlation coefficient results across all methodological combinations for the nine datasets. On average, for a given dataset, the fluctuation in RMSE (measured by standard deviation) due to changes in processing methods is 0.10 W m^{-2}. In contrast, for any given processing method, the fluctuation in RMSE due solely to switching between different datasets is 0.15 W m^{-2}. This indicates that, compared to time series processing methods, the primary source of inconsistency between current dOHC/dt estimates and CERES-EEI lies in the OHC datasets themselves. A further investigation into different types of datasets reveals that the internal spread among reanalysis datasets (RMSE of 0.15 W m^{-2}) is higher than that of the objective analysis -based datasets (RMSE of 0.12 W m^{-2}). A more comprehensive investigation on different types of data products are needed in the future.

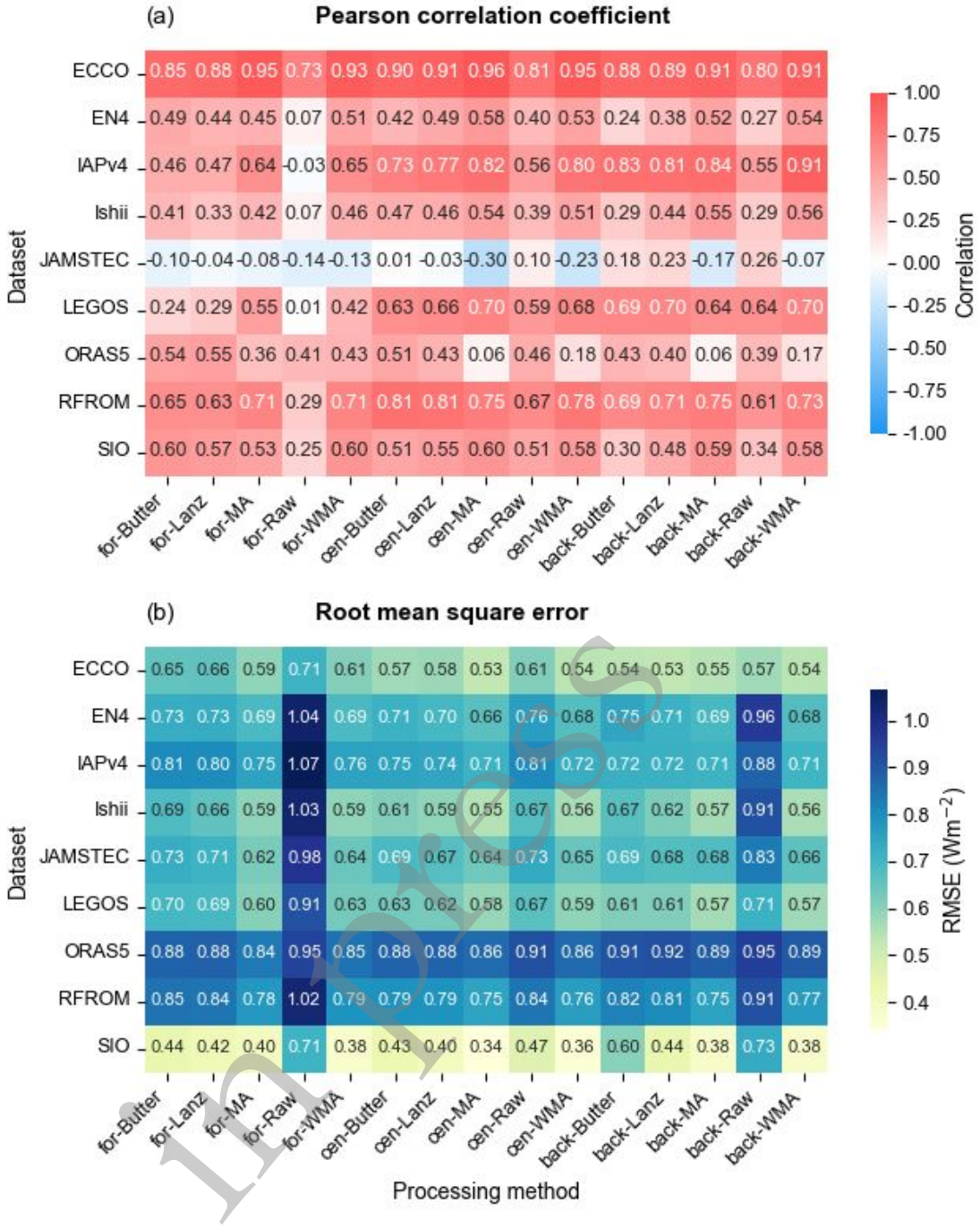

Figure 8. Summary of performance metrics for dOHC/dt estimates across all datasets and processing methods, compared with CERES-EEI. a) Heatmap of Pearson correlation coefficients. b) Heatmap of RMSE values in W m^{-2}. In both panels, each row corresponds to an OHC dataset, and each column represents one of the 15 combinations of differentiation and smoothing methods.

4. Conclusion and Discussion

This study investigates the sensitivity of dOHC/dt estimates and their consistency with CERES-EEI to the choice of time series processing methods, including smoothing, differencing, and the definition of the annual mean. The results indicate that different processing methods represent a significant source of uncertainty in dOHC/dt estimation, though their influence is secondary to the inherent differences among OHC datasets themselves. Specifically, the choice of annual mean definition introduces a 14% (calculated as the standard deviation of the trend values, 0.05 W m^{-2} $decade^{-1}$, divided by their absolute mean trend, 0.35 W m^{-2} $decade^{-1}$), relative uncertainty in the estimated long-term trend of dOHC/dt. Adopting the cross-year average definition removes some spurious interannual signals and improves the consistency between the raw ensemble mean dOHC/dt series and CERES-EEI. The choice of differencing method alters the phase and amplitude of the interannual signal in dOHC/dt and also introduces a 14% (calculated as the standard deviation of the trend values, 0.04 W m^{-2} $decade^{-1}$, divided by their absolute mean trend, 0.29 W m^{-2} $decade^{-1}$) relative trend uncertainty. The central difference method yields the strongest and most stable consistency between the calculated dOHC/dt and CERES-EEI. The choice of smoothing method has the smallest impact on the long-term trend of dOHC/dt (6% relative uncertainty) (calculated as the standard deviation of the trend values, 0.02 W m^{-2} $decade^{-1}$, divided by their absolute mean trend, 0.33 W m^{-2} $decade^{-1}$), with its

primary role being the improvement of correlation with CERES. The selection of the OHC dataset is the absolute dominant factor in the current inconsistencies between dOHC/dt and CERES-EEI. The uncertainty in RMSE introduced by dataset choice (standard deviation: 0.15 W m^{-2}) is greater than the typical uncertainty introduced by processing method choice (0.10 W m^{-2}). Furthermore, dataset selection introduces an 83% (calculated as the standard deviation of the trend values, 0.29 W m^{-2} $decade^{-1}$, divided by the mean trend, 0.35 W m^{-2} $decade^{-1}$) relative uncertainty in the estimated long-term trend of dOHC/dt. Therefore, to further improve the accuracy of dOHC/dt estimation, future efforts must not only consider data processing procedures but, more critically, aim to reduce the systematic biases among different OHC datasets.

The findings of this study lead to several actionable recommendations for future research. To obtain more reliable dOHC/dt estimates, analyses should prioritize the use of the cross-year (Jul-Jun) annual mean and adopt the center difference method, which is demonstrably superior in phase accuracy and overall error. Furthermore, smoothing is critical for improving the intercomparison between dOHC/dt and CERES-EEI, robust filters (e.g., Lanzcos, Butterworth) can be preferred.

This study primarily focuses on the uncertainty introduced by the choice of time series processing methods itself, but how these methods interact with the errors in the original data and data processing procedures, i.e., instrumental error and gap-infilling approach, is an equally important issue. All data-processing steps modulate the OHC estimate error. For example, the choice of annual mean definition, by altering the

529 combination of signals, can introduce or eliminate spurious errors (such as the peak
530 during 2016-2017 in Section 3.1).

531 Differentiation, as a high-pass filter, can amplify high-frequency noise in the input
532 data. However, the performance of different differencing schemes varies significantly.
533 The analysis in Section 3.2 shows that the interannual standard deviation produced by
534 central difference (0.27 W m^{-2}) is notably lower than that from forward (0.40 W m^{-2})
535 and backward difference (0.43 W m^{-2}). Furthermore, smoothing methods, in turn, are
536 intended to suppress errors by applying a low-pass filter, but this study's analysis
537 reveals this to be an extremely complex trade-off process. On the one hand, smoothing
538 significantly enhances the correlation with CERES. On the other hand, its contribution
539 to reducing the overall absolute error (RMSE) is quite limited (an average reduction of
540 only 0.07 W m^{-2}). This result may suggest that the dominant residual error in the
541 dOHC/dt series is not high-frequency random noise, but rather lower-frequency
542 systematic issues in data and data processing (as revealed by inter-products differences).
543 One illustrative example of this trade-off is that when the 3-year moving average (MA)
544 is applied to the JAMSTEC dataset, its correlation coefficient deteriorates sharply to -
545 0.30. This clearly demonstrates that a processing method aimed at suppressing
546 uncertainty, if mismatched with the data's characteristics, can in fact severely distort
547 the physical signal, thereby significantly amplifying the final estimation error.

548 Beyond the general discussion on error propagation, specific findings from this
549 study also highlight the close connection between physical processes and calculation

methods. The quantitative analysis in Section 3.2 shows that the backward difference method (mean r = 0.52) systematically outperforms the forward difference method (mean r = 0.07). This difference is intriguing, if not random, may have a physical explanation for instance the impacts of land/atmosphere heat storage and the ice melting energy, which might not be in phase with OHC changes. A deeper investigation into this physical mechanism presents a valuable direction for future research.

Considering that doing the time derivative can amplify errors, this study further explored whether integrating the EEI rather than differentiating it could yield better results (i.e. better consistency between OHC-EEI and CERES-EEI). Figure 9 compares the detrended OHC time series with the integrated CERES-EEI series. Before 2018, the interannual variations of most series were broadly similar; however, a systematic deviation occurred thereafter. The energy accumulation acceleration differs significantly across datasets, ranging from -0.02 to +0.81 W m^{-2} $decade^{-1}$. To further evaluate whether the integration method outperforms differencing, this study compares the uncertainty in acceleration estimates between the two approaches. The trend uncertainty among datasets (measured by standard deviation) obtained using the integration method is 0.24 W m^{-2} $decade^{-1}$, representing a reduction of approximately 17% from the 0.29 W m^{-2} $decade^{-1}$ uncertainty of the differencing method. W m^{-2} $decade^{-1}$W m^{-2} $decade^{-1}$This indicates that the integration method reduces errors by effectively suppressing noise.

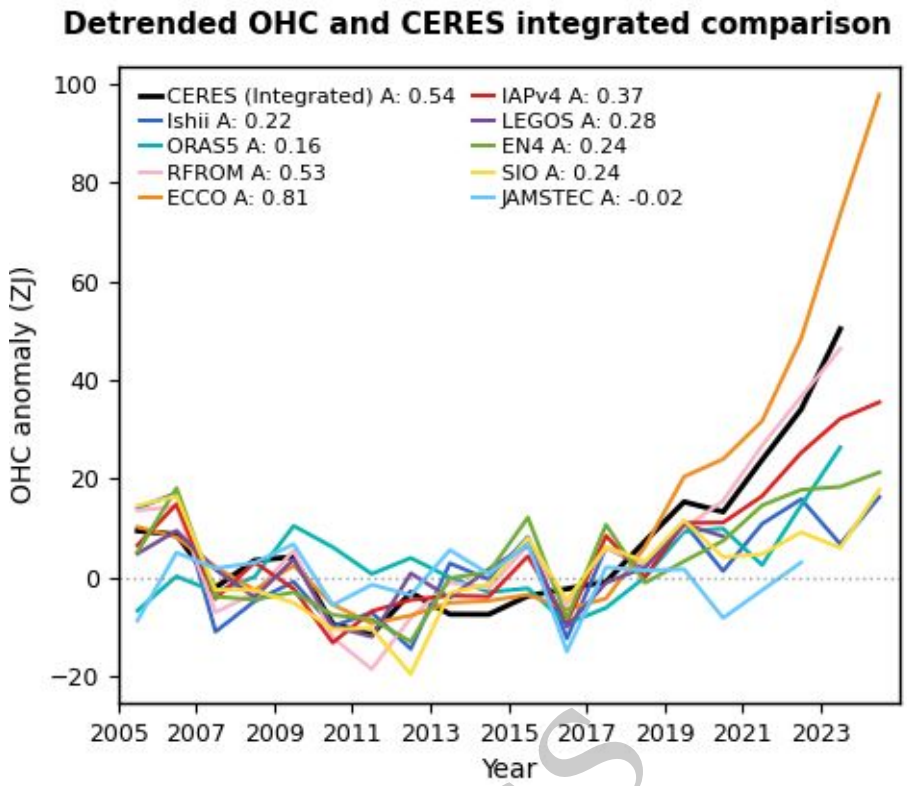

571

572 **Figure 9.** Comparison of detrended OHC anomalies from nine datasets with the
573 integrated CERES-EEI. The colored curves represent detrended OHC anomalies (in ZJ)
574 for different OHC datasets, while the solid black line shows the detrended time-
575 integrated CERES radiative flux anomalies. Results based on the Jan-Dec mean. The
576 legend value 'A' for each series is the ocean warming acceleration (in W m^{-2} $decade^{-1}$),
577 derived from a quadratic fit to the original (non-detrended) time series.

578

579 The findings of this study indicate that when comparing different OHC-based EEI
580 estimates with CERES-EEI, it is essential to fully account for the differences introduced
581 by data processing methods, such as smoothing, differencing, and the definition of the
582 annual mean. Future efforts should focus on optimizing observation systems,
583 standardizing data processing protocols, and enhancing multi-source data assimilation

584 to reduce uncertainties and improve the accuracy of dOHC/dt estimates. Addressing
585 these issues will not only enable a more precise quantification of the Earth's energy
586 budget but also provide more reliable observational constraints to help evaluate climate
587 models and reduce uncertainties in their estimates of future climate.
588
589 ***Acknowledgement.*** This study was supported by the National Key R&D Program
590 of China (Grant No. 2023YFF0806500). We thank for the technical support of the
591 National Large Scientific and Technological Infrastructure "Earth System Numerical
592 Simulation Facility" (https://cstr.cn/31134.02.EL). We acknowledge the World
593 Climate Research Programme's Working Group on Coupled Modelling, which is
594 responsible for CMIP, and we thank the climate modeling groups for producing and
595 making available their model output through the Earth System Grid Federation. Argo
596 data were collected and made freely available by the International Argo Program and
597 the national programmes contributing to it (https://argo.ucsd.edu, https://www.ocean-
598 ops.org). The Argo Program is part of the Global Ocean Observing System. We are
599 thankful to the colleagues from the National Centers for Environmental Information
600 (NCEI) and the Argo Global Assembly Center (GDAC) for providing access to the data
601 used in this study.
602 ***Data availability statement.*** The datasets utilized in this study are publicly
603 available from the following sources. The IAPv4 dataset can be accessed via
604 http://www.ocean.iap.ac.cn/pages/dataService/dataService.html?. The Ishii dataset is

available at https://climate.mri-jma.go.jp/pub/ocean/ts/v7.3.1/, and the EN4 dataset can be obtained from https://www.metoffice.gov.uk/hadobs/en4/index.html. The SIO dataset is accessible at https://sio-argo.ucsd.edu/RG_Climatology.html, while the JAMSTEC dataset is available from https://www.jamstec.go.jp/argo_research/dataset/moaagpv/moaa_en.html. For reanalysis data, the ECCO dataset can be retrieved from https://ecco-group.org/ohc.htm, and the ORAS5 dataset is available at https://www.ecmwf.int/en/forecasts/dataset/ocean-reanalysis-system-5. Among satellite-based data, the LEGOS dataset is accessible via https://earthobservation.magellium.com/project/moheacan/?lang=en, and the CERES dataset can be obtained from https://ceres.larc.nasa.gov/data/ . The fused data PMEL RFROM is available at https://www.pmel.noaa.gov/rfrom.

REFERENCES

Ablain, M., Meyssignac, B., Zawadzki, L., Jugier, R., Ribes, A., Spada, G., . . . Picot, N. (2019). Uncertainty in satellite estimates of global mean sea-level changes, trend and acceleration. *Earth System Science Data, 11*(3), 1189-1202. doi:10.5194/essd-11-1189-2019

Abraham, J. P., Baringer, M., Bindoff, N. L., Boyer, T., Cheng, L. J., Church, J. A., . . . Willis, J. K. (2013). A review of global ocean temperature observations: Implications for ocean heat content estimates and climate change. *Reviews of Geophysics, 51*(3), 450-483. doi:10.1002/rog.20022

Caron, L., Ivins, E. R., Larour, E., Adhikari, S., Nilsson, J., & Blewitt, G. (2018). GIA Model Statistics for GRACE Hydrology, Cryosphere, and Ocean Science. *Geophysical Research Letters, 45*(5), 2203-2212. doi:10.1002/2017gl076644

Cheng, L., Luo, H., Boyer, T., Cowley, R., Abraham, J., Gouretski, V., . . . Zhu, J. (2018). How Well Can We Correct Systematic Errors in Historical XBT Data? *Journal of Atmospheric and Oceanic Technology, 35*(5), 1103-1125. doi:10.1175/jtech-d-17-0122.1

633 Cheng, L., Pan, Y., Tan, Z., Zheng, H., Zhu, Y., Wei, W., . . . Zhu, J. (2024). IAPv4
634 ocean temperature and ocean heat content gridded dataset. *Earth System*
635 *Science Data, 16*(8), 3517-3546. doi:10.5194/essd-16-3517-2024
636 Cheng, L., Trenberth, K. E., Fasullo, J., Boyer, T., Abraham, J., & Zhu, J. (2017).
637 Improved estimates of ocean heat content from 1960 to 2015. *Sci Adv, 3*(3),
638 e1601545. doi:10.1126/sciadv.1601545
639 Cheng, L., von Schuckmann, K., Abraham, J. P., Trenberth, K. E., Mann, M. E.,
640 Zanna, L., . . . Lin, X. (2022a). Past and future ocean warming. *Nature*
641 *Reviews Earth & Environment, 3*(11), 776-794. doi:10.1038/s43017-022-
642 00345-1
643 Cheng, L., & Zhu, J. (2016). Benefits of CMIP5 Multimodel Ensemble in
644 Reconstructing Historical Ocean Subsurface Temperature Variations. *Journal*
645 *of Climate, 29*(15), 5393-5416. doi:10.1175/jcli-d-15-0730.1
646 Domingues, C. M., Church, J. A., White, N. J., Gleckler, P. J., Wijffels, S. E., Barker,
647 P. M., & Dunn, J. R. (2008). Improved estimates of upper-ocean warming and
648 multi-decadal sea-level rise. *Nature, 453*(7198), 1090-1093.
649 doi:10.1038/nature07080
650 Forget, G., J-M, C., P, H., CN, H., RM, P., & C, W. (2015). ECCO version 4: an
651 integrated framework for non-linear inverse modeling and global ocean state
652 estimation. *Geoscientific Model Development, 8*(10), 3071-3104.
653 doi:10.5194/gmd-8-3071-2015
654 Good, S. A., Martin, M. J., & Rayner, N. A. (2013). EN4: Quality controlled ocean
655 temperature and salinity profiles and monthly objective analyses with
656 uncertainty estimates. *Journal of Geophysical Research: Oceans, 118*(12),
657 6704-6716. doi:10.1002/2013jc009067
658 Gouretski, V., & Koltermann, K. P. (2007). How much is the ocean really warming?
659 *Geophysical Research Letters, 34*(1). doi:10.1029/2006gl027834
660 Hakuba, M. Z., Fourest, S., Boyer, T., Meyssignac, B., Carton, J. A., Forget, G., . . .
661 von Schuckmann, K. (2024). Trends and Variability in Earth's Energy
662 Imbalance and Ocean Heat Uptake Since 2005. *Surveys in Geophysics, 45*(6),
663 1721-1756. doi:10.1007/s10712-024-09849-5
664 Hakuba, M. Z., Frederikse, T., & Landerer, F. W. (2021). Earth's Energy Imbalance
665 From the Ocean Perspective (2005–2019). *Geophysical Research Letters,*
666 *48*(16). doi:10.1029/2021gl093624
667 Hansen, J., Sato, M., Kharecha, P., & von Schuckmann, K. (2011). Earth's energy
668 imbalance and implications. *Atmospheric Chemistry and Physics, 11*(24),
669 13421-13449. doi:10.5194/acp-11-13421-2011
670 Hosoda, S., & T, N. (2008). A monthly mean dataset of global oceanic temperature
671 and salinity derived from Argo float observations. *JAMSREC Rep, 8*, 47-59.
672 Ishii, M., Fukuda, Y., Hirahara, S., Yasui, S., Suzuki, T., & Sato, K. (2017). Accuracy
673 of Global Upper Ocean Heat Content Estimation Expected from Present
674 Observational Data Sets. *Sola, 13*(0), 163-167. doi:10.2151/sola.2017-030

675 Johnson, G. C., Lyman, J. M., Boyer, T., Cheng, L., Gilson, J., Ishii, M., . . . Purkey,
676 S. G. (2021). Ocean heat content. *Bull. Am. Meteorol. Soc, 102*, S156–S159.
677 doi:10.1175/
678 Kuhlbrodt, T., & Gregory, J. M. (2012). Ocean heat uptake and its consequences for
679 the magnitude of sea level rise and climate change. *Geophysical Research*
680 *Letters, 39*(18). doi:10.1029/2012gl052952
681 L'Ecuyer, T. S., Hilburn, K., Lettenmaier, D. P., Clark, E., Schlosser, C. A., Gao,
682 X., . . . Beaudoing, H. K. (2015). The Observed State of the Energy Budget in
683 the Early Twenty-First Century. *Journal of Climate, 28*(21), 8319-8346.
684 doi:10.1175/jcli-d-14-00556.1
685 Loeb, N. G., Doelling, D. R., Wang, H., Su, W., Nguyen, C., Corbett, J. G., . . . Kato,
686 S. (2018). Clouds and the Earth's Radiant Energy System (CERES) Energy
687 Balanced and Filled (EBAF) Top-of-Atmosphere (TOA) Edition-4.0 Data
688 Product. *Journal of Climate, 31*(2), 895-918. doi:10.1175/jcli-d-17-0208.1
689 Loeb, N. G., Johnson, G. C., Thorsen, T. J., Lyman, J. M., Rose, F. G., & Kato, S.
690 (2021). Satellite and Ocean Data Reveal Marked Increase in Earth's Heating
691 Rate. *Geophysical Research Letters, 48*(13). doi:10.1029/2021gl093047
692 Lyman, J. M., & GC, J. (2023). Global high-resolution random forest regression maps
693 of ocean heat content anomalies using in situ and satellite data. *J. Atmos.*
694 *Oceanic Tech., 30*(5), 575-586. doi:10.1175/JTECH-D-22-0058.1
695 Lyman, J. M., Good, S. A., Gouretski, V. V., Ishii, M., Johnson, G. C., Palmer, M.
696 D., . . . Willis, J. K. (2010). Robust warming of the global upper ocean.
697 *Nature, 465*(7296), 334-337. doi:10.1038/nature09043
698 Marti, F., Blazquez, A., Meyssignac, B., Ablain, M., Barnoud, A., Fraudeau, R., . . .
699 Benveniste, J. (2022). Monitoring the ocean heat content change and the Earth
700 energy imbalance from space altimetry and space gravimetry. *Earth System*
701 *Science Data, 14*(1), 229-249. doi:10.5194/essd-14-229-2022
702 Meyssignac, B., Boyer, T., Zhao, Z., Hakuba, M. Z., Landerer, F. W., Stammer,
703 D., . . . Zilberman, N. (2019). Measuring Global Ocean Heat Content to
704 Estimate the Earth Energy Imbalance. *Frontiers in Marine Science, 6*.
705 doi:10.3389/fmars.2019.00432
706 Palmer, M. D., Roberts, C. D., Balmaseda, M., Chang, Y. S., Chepurin, G., Ferry,
707 N., . . . Xue, Y. (2015). Ocean heat content variability and change in an
708 ensemble of ocean reanalyses. *Climate Dynamics, 49*(3), 909-930.
709 doi:10.1007/s00382-015-2801-0
710 Rasmusson, E. M., & Carpenter, T. H. (1982). Variations in Tropical Sea Surface
711 Temperature and Surface Wind Fields Associated with the Southern
712 Oscillation/El Niño. *Mon. Wea. Rev., 110*(5), 354–384.
713 doi:https://doi.org/10.1175/1520-0493(1982)110<0354:VITSST>2.0.CO;2
714 Rhein, M., & Coauthors. (2013). *2013: Observations: Ocean. Climate Change 2013 –*
715 *The Physical Science Basis: Working Group I Contribution to the Fifth*

Assessment Report of the Intergovernmental Panel on Climate Change. Cambridge: Cambridge University Press.

Roberts, C. D., Palmer, M. D., Allan, R. P., Desbruyeres, D. G., Hyder, P., Liu, C., & Smith, D. (2017). Surface flux and ocean heat transport convergence contributions to seasonal and interannual variations of ocean heat content. *Journal of Geophysical Research: Oceans, 122*(1), 726-744. doi:10.1002/2016jc012278

Roemmich, D., & Gilson, J. (2009). The 2004–2008 mean and annual cycle of temperature, salinity, and steric height in the global ocean from the Argo Program. *Progress in Oceanography, 82*(2), 81-100. doi:10.1016/j.pocean.2009.03.004

Storto, A., Masina, S., Balmaseda, M., Guinehut, S., Xue, Y., Szekely, T., . . . Wang, X. (2015). Steric sea level variability (1993–2010) in an ensemble of ocean reanalyses and objective analyses. *Climate Dynamics, 49*(3), 709-729. doi:10.1007/s00382-015-2554-9

Trenberth, K. E., Fasullo, J. T., & Kiehl, J. (2009). Earth's global energy budget. . *Bulletin of the american meteorological society, 90*(3), 311-324. doi:10.1175/2008BAMS2634.I

Trenberth, K. E., Fasullo, J. T., von Schuckmann, K., & Cheng, L. (2016). Insights into Earth's Energy Imbalance from Multiple Sources. *Journal of Climate, 29*(20), 7495-7505. doi:10.1175/jcli-d-16-0339.1

von Schuckmann, K., Minière, A., Gues, F., Cuesta-Valero, F. J., Kirchengast, G., Adusumilli, S., . . . Zemp, M. (2023). Heat stored in the Earth system 1960–2020: where does the energy go? *Earth System Science Data, 15*(4), 1675-1709. doi:10.5194/essd-15-1675-2023

von Schuckmann, K., Palmer, M. D., Trenberth, K. E., Cazenave, A., Chambers, D., Champollion, N., . . . Wild, M. (2016). An imperative to monitor Earth's energy imbalance. *Nature Climate Change, 6*(2), 138-144. doi:10.1038/nclimate2876

von Schuckmann, K., Sallée, J. B., Chambers, D., Le Traon, P. Y., Cabanes, C., Gaillard, F., . . . Hamon, M. (2014). Consistency of the current global ocean observing systems from an Argo perspective. *Ocean Science, 10*(3), 547-557. doi:10.5194/os-10-547-2014

Wiese, D. N., Landerer, F. W., & Watkins, M. M. (2016). Quantifying and reducing leakage errors in the JPL RL05M GRACE mascon solution. *Water Resources Research, 52*(9), 7490-7502. doi:10.1002/2016wr019344

Zuo, H., Balmaseda, M. A., Tietsche, S., Mogensen, K., & Mayer, M. (2019). The ECMWF operational ensemble reanalysis–analysis system for ocean and sea ice: a description of the system and assessment. *Ocean Science, 15*(3), 779-808. doi:10.5194/os-15-779-2019